Atomic layer-by-layer Co3O4/graphene composite for high performance lithium-ion batteries

Author

Dou, Yuhai, Xu, Jiantie, Ruan, Boyang, Liu, Qiannan, Pan, Yuede, Sun, Ziqi, Dou, Shi Xue

Published

2016

Journal Title

Advanced Energy Materials

Version

Accepted Manuscript (AM)

DOI

10.1002/aenm.201501835

DOI: 10.1002/((please add manuscript number))

Article type: Communication

Atomic Layer-by-Layer Co_3O_4/Graphene Composite for High Performance Lithium-Ion Batteries

Yuhai Dou, Jiantie Xu, Boyang Ruan, Qiannan Liu, Yuede Pan, Ziqi Sun, and Shi Xue Dou**

Y. Dou, Dr. J. Xu, B. Ruan, Q. Liu, Y. Pan, Dr. Z. Sun, Prof. S. X. Dou

Institute for Superconducting and Electronic Materials, Australian Institute for Innovative Materials

University of Wollongong

Wollongong, New South Wales 2500, Australia

E-mail: ziqi.sun@qut.edu.au; shi_dou@uow.edu.au

Yuhai Dou

This is the author manuscript accepted for publication and has undergone full peer review but has not been through the copyediting, typesetting, pagination and proofreading process, which may lead to differences between this version and the Version of Record. Please cite this article as doi: 10.1002/aenm.201501835.

This article is protected by copyright. All rights reserved.

Science and Technology on Surface Physics and Chemistry Laboratory

Jiangyou, Sichuan 621907, China

Dr. Z. Sun

School of Chemistry, Physics and Mechanical Engineering

Queensland University of Technology

Brisbane, Queensland 4001, Australia

Keywords: atomically-thin, layer-by-layer, Co_3O_4, anode material, lithium-ion batteries

Increasing demands for portable electronics and the growing popularity of electric vehicles (EV) have stimulated intensive studies on rechargeable lithium-ion batteries (LIBs) with high specific capacity, enhanced rate capability, long cycle life and high stability.[1] Although graphite is holding its position as the current commercial anode for LIBs, transition metal oxides have been considered among the most promising alternatives because of their higher theoretical capacity.[2] Nevertheless, metal oxide anodes usually present low rate capability and poor cycling stability due to inherently poor electronic conductivity, slow reaction kinetics and severe volume expansion during repeated discharge-charge cycles.[3] To solve these critical issues, graphene that possesses large surface area, high intrinsic electrical conductivity and excellent mechanical flexibility is normally incorporated to enhance

This article is protected by copyright. All rights reserved.

electron transfer, accelerate reaction kinetics, and alleviate volume expansion, thereby leading to improved electrochemical performance.[4,5]

Among the reported transition metal oxide/graphene composites, layer-by-layer structure has been proved to be an effective architecture for LIBs due to the strong affinity between two types of nanosheets.[6] However, it still suffers from insufficient coupling effect due to the relatively small fraction of surface atoms of metal oxides that can bond with graphene. Recently, two-dimensional inorganic graphene analogues (IGAs) with single- or few-layer stacking have become a conceptually new class of materials.[7] These species show obvious structural disorder on their surfaces, which display an increased density of states (DOS) near the Fermi level, leading to improved electrical conductivity and accelerated reaction kinetics. More importantly, they possess a huge percentage of coordinated unsaturated surface atoms due to their atomic thickness. When hybridized with graphene, these surface atoms can bond with more carbon atoms through oxygen-containing functional groups,[8] achieving an enhanced synergistic coupling effect. Therefore, it is highly desirable to develop an ideal nanostructure of “atomic layer-by-layer” transition metal oxide/graphene to deliver extraordinary electrochemical performance in LIBs.

This article is protected by copyright. All rights reserved.

Herein, as a representative, atomically-thin mesoporous Co_3O_4 nanosheets/graphene composite (ATMCNs-GE) has been successfully developed and utilized as anode material for LIBs. This atomic layer-by-layer composite delivers high discharge capacities of 2014.7 and 1134.4 mAh g^{-1} at 0.11 and 2.25 C (with 1 C equal to 890 mA g^{-1}), respectively, presents excellent rate capability, and exhibits ultra-long cycle life and enhanced cycling stability with a capacity retention of 92.1% after 2000 cycles at 2.25 C, which significantly outperforms the performances of bare ATMCNs and any existing Co_3O_4/C (including graphene, carbon nanotubes, porous carbon, *etc.*) composites. The outstanding electrochemical performance of ATMCNs-GE is mainly attributable to the atomic thickness and mesoporosity of Co_3O_4 nanosheets for adequate electrode/electrolyte contact and shortened lithium ion diffusion length; the high electrical conductivity and flexibility of graphene for enhanced electronic/ionic transportation and improved structural stability; the high specific surface area of Co_3O_4 and graphene with abundant surface atoms, mesopores, grain boundaries, edges, defects, *etc.* for extra lithium storage; as well as the unique atomic layer-by-layer structure, where the Co_3O_4 layer acts as a Li^+-accepting phase and the graphene layer as a eletron-accepting phase for reversible (pseudocapacitive) interfacial lithium storage.

Ultrathin Co_3O_4 precursor nanosheets were first synthesized via a surfactant-assisted self-assembly approach (Figure S1, see Supporting Information for details).[9] Well-crystallized

This article is protected by copyright. All rights reserved.

atomically-thin mesoporous Co_3O_4 nanosheets were then obtained after calcination at 400 °C (**Figure 1**). The scanning electron microscope (SEM) and transmission electron microscope (TEM) images (Figure 1a,b) show that the as-prepared nanosheets have a size of ~2.5 μm and possess numerous mesopores on the surface. The high-resolution TEM (HRTEM) image and corresponding fast Fourier transform (FFT) pattern of the nanosheets present a well-defined structure with lattice fringe spacings of 0.47 and 0.28 nm, associated with the (1-11) and (220) facets of cubic spinel Co_3O_4, respectively (Figure 1c).[3b,7e] Detailed structural features were characterized by employing atomic force microscopy (AFM) (Figure 1d) and surface area analysis (Figure 1e). As can be seen, a pore depth of ~2.0 nm was detected, indicating the atomic thickness of the nanosheets. These nanosheets exhibit an ultrahigh specific surface area of ~157 $m^2 g^{-1}$ and have their main pore size distribution below 12 nm.

The atomic layer-by-layer ATMCNs-GE was prepared from hybridization of ATMCNs and graphene under stirring and heating conditions (**Figure 2**a). Detailed information on ATMCNs-GE was acquired by scanning transmission electron microscopy (STEM). The STEM images clearly display the atomically-thin mesoporous Co_3O_4 nanosheets and the nearly transparent graphene nanosheets underneath (Figure 2b and c). The graphene nanosheets, ~1.2 nm in thickness, consist of 3 or 4 stacked layers, indicating an interplanar spacing of about 0.39 nm (Figure 2d). Phase characterization was then carried out by selected area

This article is protected by copyright. All rights reserved.

electron diffraction (SAED) (selected area marked by a red circle in Figure 2e). As can be seen, the SAED pattern (inset) presents the typical quasi-single-crystal feature of Co_3O_4, and some weak spots may be related to graphene. Furthermore, the elements were confirmed by energy dispersive X-ray (EDX) spectrum and energy dispersive spectroscopic (EDS) mapping. As can be seen, distinct peaks of Co, O and C were observed (Figure 2f), and homogeneously distributed Co (Figure 2g), O (Figure 2h) and C (Figure 2i) were also clearly detected. These results show that atomically-thin Co_3O_4 nanosheets and graphene were successfully hybridized with each other through layer-by-layer adhesion. The graphene content in the ATMCNs-GE was estimated by thermogravimetric analysis (TGA). As shown in Figure S2, the non-stoichiometric weight loss for ATMCNs-GE is about 5.8% compared with that of ATMCNs, indicating that 5.8 wt.% graphene has been incorporated.

The atomic layer-by-layer structure of ATMCNs-GE was further studied by X-ray diffraction (XRD), Raman spectroscopy and X-ray photoelectron spectroscopy (XPS). The XRD pattern of graphene shows a strong peak at 22.2°, corresponding to an interplanar d_{002}-spacing of 0.395 nm (**Figure 3**a),[6d] which is consistent with the HRTEM result (Figure 2c). All diffraction peaks of ATMCNs match well with cubic spinel Co_3O_4.[3b] These peaks show very weak intensities due to the lack of long-range order in the third dimension for the atomically-thin nanosheets. For ATMCNs-GE, there is no obvious graphene peak at 22.2°, suggestive of less

This article is protected by copyright. All rights reserved.

restacking of graphene layers after hybridization with Co_3O_4 nanosheets. The Raman spectrum (Figure 3b) of ATMCNs shows two peaks at 193 and 520 cm^{-1}, ascribed to the F_{2g} mode vibration, while the peaks at 480 and 680 cm^{-1} are assigned to the E_g and A_{1g} mode vibrations, respectively.[10] The graphene nanosheets display typical D-band (due to defects, edges, or structural disorders) and G-band (first-order scattering of the E_{2g} mode observed for sp^2 carbon domains) structures.[11] As expected, these typical Raman peaks are strongly observed in ATMCNs-GE. Nevertheless, the intensity ratio of the D band to the G band (I_D/I_G, 1.46) is higher than that of graphene (1.08), indicating the increased degree of disorder (with more defects and edges exposed) for the graphene in ATMCNs-GE.[11a,b] In addition, the G band of ATMCNs-GE shows an obvious 10 cm^{-1} shift to lower wavenumber compared with that of graphene, which indicates that an interfacial charge transfer has occurred, confirming the strong coupling effect between the Co_3O_4 nanosheets and the graphene nanosheets.[11b] The XPS survey spectrum of ATMCNs-GE reveals the presence of cobalt, oxygen and carbon (Figure 3c). Figure 3d shows the O 1s XPS spectrum of graphene, in which the peak at 531.9 eV is assigned to C=O groups, while the one at 534.2 eV is ascribed to C-OH and/or C-O-C groups (hydroxyl and/or epoxy). The peak for ATMCNs at 529.2 eV corresponds to the Co-O species, and that at 531.6 eV originates from low-coordinated oxygen defects or vacancies (Figure 3e).[12] Compared with the O 1s peaks of graphene and

This article is protected by copyright. All rights reserved.

ATMCNs, there is an extra peak located at 530.2 eV for ATMCNs-GE (Figure 3f), which should be ascribed to the formation of Co-O-C linkage through the oxygen-containing functional groups of graphene. We suggest that the formation mechanism of Co-O-C linkage is similar to that of Ni-O-C, which has been studied by the first-principles calculations performed by Cheng's group.[8] Take hydroxyl groups for example, two states with minimum adsorption energy can be observed when a metal atom approaches the -OH groups on the graphene surfaces. The first is where the metal atom bonds with two O atoms and pushes aside one H atom to the surface forming a C-H bond, the second is where the metal atom bonds with three O atoms after crowding out two H atoms to form a H_2 molecule. Besides, the large energy barrier for the detachment of metal atom from oxygen atoms also indicates the formation of metal-O-C linkage. This Co-O-C linkage further suggests that the atomically-thin Co_3O_4 nanosheets and the graphene nanosheets are strongly hybridized with each other.

The electrochemical performance of the atomic layer-by-layer ATMCNs-GE as anode material was evaluated with Li insertion/extraction in the voltage range of 0.01–3.0 V. **Figure 4**a presents the cyclic voltammograms (CVs) of ATMCNs-GE at a scanning rate of 0.05 mV s^{-1}. The first cycle voltammogram features a shoulder peak at 1.10 V, attributed to the reduction of Co^{3+} to Co^{2+}, and the main cathodic peak at 0.85 V is related to the reduction of Co^{2+} to Co and the formation of the solid electrolyte interphase (SEI) film.[13] The anodic

This article is protected by copyright. All rights reserved.

peak at 2.06 V represents the oxidation of Co to CoO. In the following cycles, the ATMCNs-GE exhibits much stronger and more stable cathodic and anodic peaks compared with ATMCNs (Figure S3 and S4), illustrating higher lithium storage density and easier lithium insertion/extraction reaction. Figure 4b presents the discharge/charge voltage profiles of ATMCNs-GE at various C-rates. As can be seen, the discharge/charge plateau is increasingly shortened with increasing C-rate due to the increase in ohmic resistance and the limitation of lithium diffusion, but it is still apparent at high current densities (such as 2.25 and 5.62 C) compared with that of ATMCNs (Figure S5), indicating that less electrode polarization occurs for this hybridized structure.[14]

The rate performance at stepwise C-rates from 0.11 to 5.62 C was shown in Figure 4c. The average discharge capacities of ATMCNs-GE at 0.11, 0.22, 0.56, 1.12, 2.25 and 5.62 C are 1266.9, 1213.7, 1111.2, 978.0, 793.1 and 509.3 mAh g^{-1}, respectively. However, they are only 1172.8, 927.7, 514.9, 218.1, 91.5 and 36.4 mAh g^{-1}, respectively, for ATMCNs. Therefore, ATMCNs-GE exhibits much higher rate capability compared with ATMCNs. It is also important to note that when the current density returns to 0.11 C, ATMCNs-GE delivers an increasing reversible capacity that reaches 2014.7 mAh g^{-1} after 88 cycles, which is actually 74.1% higher than its initial discharge capacity (1157.3 mAh g^{-1}).

This article is protected by copyright. All rights reserved.

The long cycling performance at a high current density of 2.25 C was then investigated (Figure 4d). As can be seen, the capacities of ATMCNs-GE and ATMCNs suffer obvious fluctuations, which are common phenomena in transition metal oxides for LIBs.[15] The fluctuation at the beginning is mainly attributed to the formation of the SEI film, and the activation process with the lithium-ion diffusion path gradually established in the electrode.[16] The fluctuation in the extended cycles can be ascribed to the unstability of the SEI film, the electrolyte degradation, and the reaction of oxygen-containing functional groups on the graphene with lithium ions.[5f] ATMCNs-GE delivers an initial discharge capacity of 975.4 mAh g^{-1} at 2.25 C, and then experiences a quick activation process, with the discharge capacity reaching a peak value of 1134.4 mAh g^{-1} after 257 cycles. It still maintains a high capacity retention of 92.1% (851.5 mAh g^{-1}, charge capacity) after 2000 cycles compared with its initial capacity (924.8 mAh g^{-1}), indicating ultra-long cycle life and excellent cycling stability. The Coulombic efficiency (CE) rises from 94.8% in the first cycle to about 99.7% after 300 cyles, further confirming the high reversibility and outstanding cycling stability. By contrast, ATMCNs delivers an initial discharge capacity of 651.3 mAh g^{-1}, and then suffers a rapid decline in the following 10 cycles, which results from the formation of the SEI film. A long time is needed to finish the activation process, with the capacity reaching a peak value of 521.7 mAh g^{-1} after 730 cycles. After that, the capacity decreases gradually, with only

This article is protected by copyright. All rights reserved.

47.3% retention after 2000 cycles. In addition, the CE of ATMCNs is relatively unstable compared with that of ATMCNs-GE in the initial 300 cycles. More noteworthy, in the full activation state, *e.g.* the 800th cycle, ATMCNs-GE delivers a discharge capacity of 1092.8 mAh g^{-1}, which is actually 131.5% higher than the total sum of the individual capacities of ATMCNs and graphene (500.6 × 94.2% + 7.8 × 5.8% = 472.0 mAh g^{-1}), indicating the significant synergistic coupling effect brought by the Co-O-C bridge between ultrathin Co_3O_4 nanosheets and graphene nanosheets.

Electrochemical impedance spectroscopy (EIS) was further performed to understand the superior cycling performance of ATMCNs-GE (Figure S6). The impedance curves after different numbers of cycles (Figure S6a and b) clearly show the charge transfer resistance (R_{ct}), which is a key indicator for the kinetics of the electrode and is calculated from the equivalent circuit shown in the inset of Figure S5a.[17] As the fitting results show in Figure S6c, the R_{ct} of ATMCNs decreases from before cycling to the 800th cycle, and then slowly increases over the next 1200 cycles. The decrease in R_{ct} is mainly attributed to the electrode-electrolyte activation with enhanced electrical conductivity and shortened lithium-ion diffusion, and the increase in R_{ct} is ascribed to the formation of unstable and thick SEI film with worsened reaction kinetics. By contrast, ATMCNs-GE presents a more significant decrease from before cycling to the 200th cycle, which reveals a faster activation

This article is protected by copyright. All rights reserved.

process compared with ATMCNs. After that, R_{ct} remains almost constant for the subsequent 1800 cycles, suggestive of excellent cycling stability. Generally, ATMCNs-GE has much smaller electronic resistance (R_e), electrolyte resistance (R_s) and R_{ct} values than ATMCNs at corresponding cycles, indicating smaller internal resistance, a more stable SEI film (Figure S7) and improved reaction kinetics.[18]

It is important to note that the atomic layer-by-layer ATMCNs-GE exhibits superior electrochemical performance compared with previously reported Co_3O_4/C (including graphene, carbon nanotubes, porous carbon, *etc.*) composites. As can be seen in Figure 4e, the specific capacity of ATMCNs-GE reaches 2014.7 mAh g^{-1} at 0.11 C, which significantly outperforms the theoretical capacity (890 mAh g^{-1}) and the reported results obtained at C-rates of 0.028–1.1 C (see Supporting Information for details).[19] In addition, the cycle number of ATMCNs-GE exceeds 2000 with a high capacity retention at 2.25 C, far beyond those of reported Co_3O_4/C composites at 0.56–5 C.[20] The excellent electrochemical performance of ATMCNs-GE with ultrahigh specific capacity, excellent rate capability and ultra-long cycle life is mainly attributable to the following reasons. Firstly, the atomic thickness and mesoporosity of Co_3O_4 nanosheets provide large fraction of surface atoms and highly accessible surface areas. Therefore, the electrode is in full contact with the electrolyte and the lithium diffusion path is distinctly shortened.[4,7e] Secondly, the

This article is protected by copyright. All rights reserved.

incorporation of graphene not only improves the electronic conductivity, but also alleviates the volume expansion and structure degradation of Co_3O_4, which contributes greatly to the rate capability and cycling stability.[5] Thirdly, the strong connection between Co_3O_4 and graphene through the Co-O-C linkage effectively avoids the agglomeration of Co_3O_4 and the restacking of graphene during the preparation process and the deep cycling, and therefore significantly increases the utilization of active sites (*e.g.* abundant surface atoms, mesopores, grain boundaries, edges, defects, structural disorders) for extra lithium storage.[16,21] Fourthly, the unique atomic layer-by-layer structure provides notable (pseudocapacitive) interfacial storage between the two nanosheets, in which the Co_3O_4 layer acts as a Li^+-accepting phase and the graphene layer as an electron-accepting phase.[22] This synergistic interfacial storage further improves the specific capacity and the rate capability.

In conclusion, an atomic layer-by-layer structure of Co_3O_4/graphene was successfully fabricated and used as anode material for LIBs. This unique structure delivers ultrahigh specific capacities of 2014.7 and 1134.4 mAh g^{-1} at 0.11 and 2.25 C, respectively, presents excellent rate capability, and exhibits ultra-long cycle life up to 2000 cycles without obvious capacity fading at 2.25 C, far beyond the performances of bare Co_3O_4 nanosheets and any previously reported Co_3O_4/C composites. We believe that this atomic layer-by-layer

This article is protected by copyright. All rights reserved.

structure design can be extended to other IGA/graphene or IGA/IGA composites for a broad range of applications such as nanoelectronics, batteries, supercapacitors, and catalysts *etc.*

Experimental Section

Preparation of ATMCNs, graphene, and ATMCNs-GE: 0.2 g polyethylene oxide–polypropylene oxide–polyethylene oxide (PEO_{20}-PPO_{70}-PEO_{20}, Pluronic P123) was first dissolved in 3 g ethanol, then 2.5 g H_2O and 12 ml ethylene glycol (EG) were added to form a homogeneous solution. Next, 0.125 g $Co(Ac)_2{\cdot}4H_2O$ and 0.07 g hexamethylenetetramine (HMTA) were added into the mixed solution under vigorous stirring for 30 min. After that, the solution was transferred into a 45 ml autoclave and heated at 170 °C for 15 h. ATMCNs was finally obtained by calcinating the precursor at 400 °C for 1 h. Mildly oxidized graphene was synthesized by a Hummers method. For the preparation of ATMCNs-GE, the ultrathin Co_3O_4 nanosheets and mildly oxidized graphene were first dispersed in an ethanol/water (1:1, v/v) mixed solution under ultrasonic treatment. They were then transferred onto a hotplate stirrer and stirred overnight at 70 °C. Next, L-ascorbic acid was added to reduce the mildly oxidized graphene under stirring at room temperature for 24 h. After that, the hybrid powders were centrifugated and washed with water and ethonal for three times. Finally, ATMCNs-GE was obtained after drying at 60 °C. The ATMCNs and the graphene were also treated following the same procedure for comparison.

This article is protected by copyright. All rights reserved.

Characterizations: The morphology and crystal structure of the as-prepared products were observed with a scanning electron microscope (JSM-7500FA, JEOL, Tokyo, Japan) and a transmission electron microscope (JEM-2011F, JEOL, Tokyo, Japan) operated at 200 kV. Scanning transmission electron microscope (STEM) images were acquired on a probe-corrected JEOL ARM200F operated at 200 kV equipped with a cold field emission gun, a high resolution pole-piece, and a Centurio EDS detector. Images and EDS maps were acquired at a probe current of 90 pA. The elemental mapping was carried out by energy dispersive X-ray spectroscopy (EDS) using the JEOL ARM200F. Atomic force microscopy (AFM, MPF-3D, Asylum Research, Santa Barbara, USA) was applied to determine the thickness of the Co_3O_4 nanosheets. Surface area was measured by a surface area analyzer (NOVA1000, Quantachrome Co., FL, USA) at 77 K. Before measurement, the sample was degassed at 120 °C for 5 h under vacuum. Thermogravimetric analysis (TGA, TA Instruments 2000) was performed to estimate the graphene content in the composite under air atomosphere with a temperature ramp of 5 °C min^{-1} in the range of 30–700 °C. X-ray diffraction (XRD, MMA, GBC Scientific Equipment LLC, Hampshire, IL, USA) was utilized to evaluate the phases of the products. Raman spectra were collected using a Raman spectrometer (Lab RAM HR, Horiba Jobin Yvon SAS). The bonding between two nanosheets was determined by X-ray photoelectron spectroscopy (XPS, PHOIBOS 100 Analyser from SPECS, Berlin, Germany; Al K_α X-rays).

Electrochemical measurements: To prepare the anodes, ATMCNs-GE, ATMCNs or graphene was first blended with acetylene black carbon and PVDF in a weight ratio of 8:1:1, respectively. N-methyl-2-pyrrolidone (NMP) was added during the grinding process. The obtained slurry was then

This article is protected by copyright. All rights reserved.

brushed and coated on Cu foil, and dried at 120 °C for 12 h under vacuum. After that, the anode materials were taken out and pressed at a pressure of 2 MPa. The mass loadings of active material were about 0.45 mg cm^{-2}. Finally, CR 2032 coin-type cells were assembled under Ar atomosphere using the ATMCNs-GE, ATMCNs or graphene electrode as the working electrode, porous polypropylene film as the separator, and Li foil as the counter and reference electrode. 1 M $LiPF_6$ in a mixture of ethylene carbonate (EC) and diethyl carbonate (DEC) (1:1, v/v) was chosen as the electrolyte. The cells were measured using an automatic battery tester system (Land®, China) and galvanostatically discharged and charged at various current densities in the voltage range of 0.01–3.0 V. Cyclic voltammetry (CV) and electrochemical impedance spectroscopy (EIS) were conducted using a Biologic VPM3 electrochemical workstation.

Supporting Information

Supporting Information is available from the Wiley Online Library or from the author.

Acknowledgements

Y. Dou is supported by the Australian Postgraduate Award (APA), the International Postgraduate Research Scholarship (IPRS), and the Automotive CRC 2020 project 1-111. Z. Sun thanks the Australian Research Council for his DECRA Grant (DE150100280). We are also grateful to Mr. Hongqiang Wang and Mr. Feng Xiao for their help on cell assembly and AFM characterization, respectively. Y. Dou and J. Xu contributed equally to this work.

This article is protected by copyright. All rights reserved.

References

[1] a) V. Etacheri, R. Marom, R. Elazari, G. Salitra, D. Aurbach, *Energy Environ. Sci.* **2011**, *4*, 3243; b) J. B. Goodenough, Y. Kim, *Chem. Mater.* **2010**, *22*, 587; c) Y.-G. Guo, J.-S. Hu, L.-J. Wan, *Adv. Mater.* **2008**, *20*, 2878; d) C. Liu, F. Li, L.-P. Ma, H.-M. Cheng, *Adv. Mater.* **2010**, *22*, E28.

[2] a) P. Poizot, S. Laruelle, S. Grugeon, L. Dupont, J.-M. Tarascon, *Nature* **2000**, *407*, 496; b) P. G. Bruce, B. Scrosati, J.-M. Tarascon, *Angew. Chem. Int. Ed.* **2008**, *47*, 2930; c) A. S. Arico, P. Bruce, B. Scrosati, J.-M. Tarascon, W. V. Schalkwijk, *Nature Mater.* **2005**, *4*, 366; d) M. V. Reddy, G. V. S. Rao, B. V. R. Chowdari, *Chem. Rev.* **2013**, *113*, 5364; e) Y. Li, B. Tan, Y. Wu, *Nano Lett.* **2008**, *8*, 265.

[3] a) K. T. Nam, D. W. Kim, P. J. Yoo, C.-Y. Chiang, N. Meethong, P. T. Hammond, Y.-M. Chiang, A. M. Belcher, *Science* **2006**, *312*, 885; b) J. Wang, N. Yang, H. Tang, Z. Dong, Q. Jin, M. Yang, D. Kisailus, H. Zhao, Z. Tang, D. Wang, *Angew. Chem. Int. Ed.* **2013**, *52*, 6417; c) P. L. Taberna, S. Mitra, P. Poizot, P. Simon, J.-M. Tarascon, *Nature Mater.* **2006**, *5*, 567.

[4] a) H. Wang, L.-F. Cui, Y. Yang, H. S. Casalongue, J. T. Robinson, Y. Liang, Y. Cui, H. Dai, *J. Am. Chem. Soc.* **2010**, *132*, 13978; b) H. Ren, R. Yu, J. Wang, Q. Jin, M. Yang, D. Mao, D. Kisailus, H. Zhao, D. Wang, *Nano Lett.* **2014**, *14*, 6679; c) J.-M. Tarascon, M. Armand, *Nature* **2001**, *414*, 359; d) X. W. Lou, C. M. Li, L. A. Archer, *Adv. Mater.* **2009**, *21*, 2536; e) S. Ko, J.-I. Lee, H. S. Yang, S. Park, U. Jeong, *Adv. Mater.* **2012**, *24*, 4451; f) W.-M. Zhang, X.-

This article is protected by copyright. All rights reserved.

L. Wu, J.-S. Hu, Y.-G. Guo, L.-J. Wan, *Adv. Funct. Mater.* **2008**, *18*, 3941; g) H.-X. Zhang, C. Feng, Y.-C. Zhai, K.-L. Jiang, Q.-Q. Li, S.-S Fan, *Adv. Mater.* **2009**, *21*, 2299; h) R. Huang, L. Wang, Q. Zhang, Z. Chen, Z. Li, D. Pan, B. Zhao, M. Wu, C. M. L. Wu, C.-H. Shek, *ACS Nano* **2015**, *9*, 11351.

[5] a) L. Wang, D. Wang, Z. Dong, F. Zhang, J. Jin, *Nano Lett.* **2013**, *13*, 1711; b) M. Pumera, *Energy Environ. Sci.* **2011**, *4*, 668; c) J. Lin, Z. Peng, C. Xiang, G. Ruan, Z. Yan, D. Natelson, J. M. Tour, *ACS Nano* **2013**, *7*, 6001; d) X. Xin, X. Zhou, J. Wu, X. Yao, Z. Liu, *ACS Nano* **2012**, *6*, 11035; e) G. Zhou, D.-W. Wang, F. Li, L. Zhang, N. Li, Z.-S. Wu, L. Wen, G. Q. Lu, H.-M. Cheng, *Chem. Mater.* **2010**, *22*, 5306; f) W. Wei, S. Yang, H. Zhou, I. Lieberwirth, X. Feng, K. Mullen, *Adv. Mater.* **2013**, *25*, 2909; g) W. Li, F. Wang, S. Feng, J. Wang, Z. Sun, B. Li, Y. Li, J. Yang, A. A. Elzatahry, Y. Xia, D. Zhao, *J. Am. Chem. Soc.* **2013**, *135*, 18300.

[6] a) Y. Zou, Y. Wang, *Nanoscale* **2011**, *3*, 2615-2620; b) J. Kan, Y. Wang, *Sci. Rep.* **2013**, *3*, 3502; c) X.-l. Huang, R.-z. Wang, D. Xu, Z.-l. Wang, H.-g. Wang, J.-j. Xu, Z. Xu, Q.-c. Liu, Y. Zhang, X.-b. Zhang, *Adv. Funct. Mater.* **2013**, *23*, 4345; d) S. Q. Chen, Y. Wang, *J. Mater. Chem.* **2010**, *20*, 9735.

[7] a) Y. Du, Z. Yin, J. Zhu, X. Huang, X.-J. Wu, Z. Zeng, Q. Yan, H. Zhang, *Nat. Commun.* **2012**, *3*, 1177; b) M. Chhowalla, H. S. Shin, G. Eda, L.-J. Li, K. P. Loh, H. Zhang, *Nature Chem.* **2013**, *5*, 263; c) Y. Sun, S. Gao, Y. Xie, *Chem. Soc. Rev.* **2014**, *43*, 530; d) X. Zhang, Y.

This article is protected by copyright. All rights reserved.

Xie, *Chem. Soc. Rev.* **2013**, *42*, 8187; e) J. Zhu, L. Bai, Y. Sun, X. Zhang, Q. Li, B. Cao, W. Yan, Y. Xie, *Nanoscale* **2013**, *5*, 5241.

[8] G. Zhou, D.-W. Wang, L.-C. Yin, N. Li, F. Li, H.-M. Cheng, *ACS Nano* **2012**, *6*, 3214.

[9] Z. Sun, T. Liao, Y. Dou, S. M. Hwang, M.-S. Park, L. Jiang, J. H. Kim, S. X. Dou, *Nat. Commun.* **2014**, *5*, 3813.

[10] H. Kim, D.-H. Seo, S.-W. Kim, J. Kim, K. Kang, *Carbon* **2011**, *49*, 326.

[11] a) Y. Zhan, B. Zhang, L. Cao, X. Wu, Z. Lin, X. Yu, X. Zhang, D. Zeng, F. Xie, W. Zhang, J. Chen, H. Mweng, *Carbon* **2015**, *94*, 1. b) J. Xu, I.-Y. Jeon, J.-M. Seo, S. Dou, L. Dai, J.-B. Baek, *Adv. Mater.* **2014**, *26*, 7317; c) S. Zhang, W. Li, B. Tan, S. Chou, Z. Li, S. X. Dou, *J. Mater. Chem. A* **2015**, *3*, 4793.

[12] a) L. Zhang, W. He, X. Xiang, Y. Li, F. Li, *RSC Adv.* **2014**, *4*, 43357; b) D. Li, D. Yang, X. Zhu, D. Jing, Y. Xia, Q. Ji, R. Cai, H. Li, Y. Che, *J. Mater. Chem. A* **2014**, *2*, 18761.

[13] a) L. Luo, J. Wu, J. Xu, V. P. Dravid, *ACS Nano* **2014**, *8*, 11560; b) Q. Su, J. Zhang, Y. Wu, G. Du, *Nano Energy* **2014**, *9*, 264.

[14] J. Chen, L. Yang, S. Fang, S.-i. Hirano, K. Tachibana, *J. Power Sources* **2012**, *200*, 59.

[15] H. Sun, G. Xin, T. Hu, M. Yu, D. Shao, X. Sun, J. Lian, *Nature Commun.* **2014**, *5*, 4526.

[16] Z.-S. Wu, W. Ren, L. Xu, F. Li, H.-M. Cheng, *ACS Nano* **2011**, *5*, 5463.

[17] L. Li, A.-R. O. Raji, J. M. Tour, *Adv. Mater.* **2013**, *25*, 6298.

This article is protected by copyright. All rights reserved.

[18] J. Xu, J. Shui, J. Wang, M. Wang, H.-K. Liu, S. X. Dou, I.-Y. Jeon, J.-M. Seo, J.-B. Baek, L. Dai, *ACS Nano* **2014**, *8*, 10920.

[19] a) Z.-S. Wu, W. Ren, L. Wen, L. Gao, J. Zhao, Z. Chen, G. Zhou, F. Li, H.-M. Cheng, *ACS Nano* **2010**, *4*, 3187; b) Y. Wang, H. J. Zhang, L. Lu, L. P. Stubbs, C. C. Wong, J. Lin, *ACS Nano* **2010**, *4*, 4753; c) D. Gu, W. Li, F. Wang, H. Bongard, B. Spliethoff, W. Schmidt, C. Weidenthaler, Y. Xia, D. Zhao, F. Schuth, *Angew. Chem. Int. Ed.* **2015**, *54*, 7060.

[20] a) H. Wang, N. Mao, J. Shi, Q. Wang, W. Yu, X. Wang, *ACS Appl. Mater. Interfaces* **2015**, *7*, 2882; b) L. Shen, C. Wang, *Electrochim. Acta* **2014**, *133*, 16.

[21] a) D. Pan, S. Wang, B. Zhao, M. Wu, H. Zhang, Y. Wang, Z. Jiao, *Chem. Mater.* **2009**, *21*, 3136; b) H. Hwang, H. Kim, J. Cho, *Nano Lett.* **2011**, *11*, 4826; c) J. Zhou, J. Qin, X. Zhang, C. Shi, E. Liu, N. Zhao, C. He, *ACS Nano* **2015**, *9*, 3837.

[22] a) R. Liu, S. Zhao, M. Zhang, F. Feng, Q. Shen, *Chem. Commun.* **2015**, *51*, 5728; b) W. Kang, Y. Tang, W. Li, X. Yang, H. Xue, Q. Yang, C.-S. Lee, *Nanoscale* **2015**, *7*, 225; c) C. Chen, Y. Wen, X. Hu, X. Ji, M. Yan, L. Mai, P. Hu, B. Shan, Y. Huang, *Nature Commun.* **2015**, *6*, 6929; d) J.-Y. Shin, D. Samuelis, J. Maier, *Adv. Funct. Mater.* **2011**, *21*, 3464; e) J. Maier, *Angew. Chem. Int. Ed.* **2013**, *52*, 4998.

An "atomic layer-by-layer" structure of Co_3O_4/graphene was developed as an anode material for LIBs. Due to the atomic thickness of both the Co_3O_4 nanosheets and the graphene, the

This article is protected by copyright. All rights reserved.

composite exhibits an ultrahigh specific capacity of 1134.4 mAh g^{-1} and an ultra-long life up to 2000 cycles at 2.25 C, far beyond the performances of previously reported Co_3O_4/C composites.

Keywords: atomically-thin, layer-by-layer, Co_3O_4, anode material, lithium-ion batteries

Yuhai Dou, Jiantie Xu, Boyang Ruan, Qiannan Liu, Yuede Pan, Ziqi Sun, and Shi Xue Dou**

Atomic Layer-by-Layer Co_3O_4/Graphene for High Performance Lithium-Ion Batteries

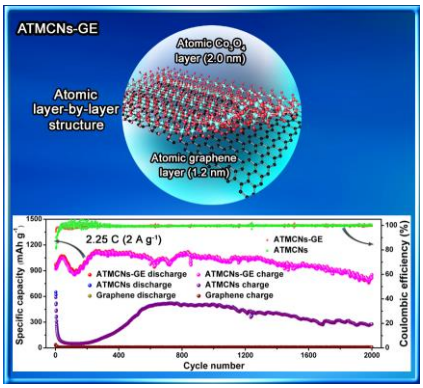

This article is protected by copyright. All rights reserved.

Figure Captions

Figure 1. Atomically-thin mesoporous Co_3O_4 nanosheets (ATMCNs). a, SEM image of ATMCNs. **b**, TEM image of a typical mesoporous Co_3O_4 nanosheet. **c**, HRTEM image of the Co_3O_4 nanosheets and its corresponding FFT pattern (inset). **d**, AFM image and height profile (inset) for the nanosheets. **e**, N_2 adsorption-desorption isotherms and pore size distribution

This article is protected by copyright. All rights reserved.

(inset). Scale bars: 2 μm (**a**), 1 μm (**b**) and 2 nm (**c**).

Figure 2. Preparation and STEM images of atomic layer-by-layer ATMCNs-GE. a, Schematic drawing for the preparation of ATMCNs-GE. **b**, **c**, Low-magnification STEM images of ATMCNs-GE. **d**, High-resolution STEM image. **e**, STEM image with corresponding SAED pattern of circled area (inset). **f**, EDX spectrum. Corresponding element mappings of **e**: cobalt (**g**); oxygen (**h**); and carbon (**i**).

Figure 3. Characterizations of atomic layer-by-layer ATMCNs-GE. a, XRD patterns of ATMCNs-GE, ATMCNs and graphene. **b**, Raman spectra of ATMCNs-GE, ATMCNs and graphene, with the inset showing details of the G band. **c**, XPS survey spectra of ATMCNs-GE, ATMCNs and graphene. O 1s XPS spectra for graphene (**d**), ATMCNs (**e**) and ATMCNs-GE (**f**).

Figure 4. Electrochemical performance of atomic layer-by-layer ATMCNs-GE in LIBs. a, CV curves for the first 5 cycles of ATMCNs-GE electrode at a scanning rate of 0.05 mV s^{-1}. **b**, Discharge-charge profiles of ATMCNs-GE at various C-rates. **c**, Rate capabilities and capacity ratio (inset) of ATMCNs-GE and ATMCNs. **d**, Cycling performances and CEs of ATMCNs-GE, ATMCNs and graphene at a high current density of 2.25 C. **e**, Comparisons of specific capacity and cycling performance between ATMCNs-GE and previously reported Co_3O_4/C (including graphene, carbon nanotubes, porous carbon, *etc.*) composites (black balls for

This article is protected by copyright. All rights reserved.

capacity comparison were obtained at 0.028–1.1 C, blue balls for cycling performance comparison were obtained at 0.56–5 C).

This article is protected by copyright. All rights reserved.